Infrared emission bands and thermal effects for 440-nm-emitting GaN-based laser diodes

Cite as: AIP Advances 10, 055311 (2020); doi: 10.1063/1.5143802
Submitted: 10 March 2020 • Accepted: 25 April 2020 •
Published Online: 12 May 2020

Feng Mao,[1] Jin Hong,[1] Han Wang,[1] Ye Chen,[1] Chengbin Jing,[1] Pingxiong Yang,[1] Jens W. Tomm,[2,a] Junhao Chu,[1,3] and Fangyu Yue[1,b]

AFFILIATIONS

[1]Key Laboratory of Polar Materials and Devices, East China Normal University, 200241 Shanghai, People's Republic of China
[2]Max-Born-Institut für Nichtlineare Optik und Kurzzeitspektroskopie, Max-Born-Str. 2A, 12489 Berlin, Germany
[3]National Laboratory for Infrared Physics, Shanghai Institute of Technical Physics, Shanghai 200083, People's Republic of China

[a]**Electronic mail:** tomm@mbi-berlin.de
[b]**Author to whom correspondence should be addressed:** fyyue@ee.ecnu.edu.cn

ABSTRACT

Broad emission bands due to defects in (In,Ga,Al)N laser diodes operating at 440 nm are investigated using continuous-wave and pulsed currents. In addition to known yellow–green and short-wave infrared bands, defect emissions were observed even in the medium-wave infrared range. A separation from thermal radiation is possible. When using pulsed currents, a super-linearly increasing emission occurs at ~1150 nm, which could be attributed to amplified spontaneous emission mainly due to the electroluminescence of deep defects in the optically active region. These results may be useful in interpreting the output power bottleneck of GaN-based lasers compared to mature GaAs-based lasers.

GaN-based laser diodes (LDs) are on track to becoming the major source of photonic power in the blue–green spectral region.[1] Currently, they suffer from an efficiency drop at high current densities, limiting the output power to several watts (single chip), far below those of mature GaAs-based LDs (up to hundreds of watts per single chip).[2] One of the main reasons is attributed to the abundant defects in the GaN base material.[3] These defects, of course, produce all the residual emissions in addition to the desired laser line. Spontaneous edge emissions can occur from materials that are part of the epitaxial architecture, such as barriers or waveguides.[4] Transitions via states generated by defects in the active region,[5] waveguide,[6] or the substrate[7,8] are further potential sources. In earlier studies, we investigated the microscopic origin of transitions such as the very intense yellow emission at ~580 nm[9] and the short-wave infrared (SWIR) emission[10] for 450 nm GaN-based devices using continuous-wave (cw) currents.

Here, we investigate broad defect emissions and the operation-induced thermal radiation of 440 nm GaN-based LDs operated with cw and pulsed currents. The results show that, in addition to the well-known yellow–green and SWIR emissions, genuine defect emissions can extend into the medium-wave infrared (MWIR) region and can be separated from thermal radiation. More interestingly, SWIR defects can produce amplified spontaneous emission (ASE) peaking at ~1150 nm when pulsed currents are applied. By comparing the emissions with the photoluminescence (PL) from a pure GaN substrate, the origin and the cause of this deep defect-related ASE are discussed and interpreted. The results could provide insights into the output power bottleneck of GaN-based LDs and help in enhancing the stability of the devices.

LDs emit at a wavelength of 440 nm. Their epitaxial architecture is based on an (In,Ga,Al)N sequence of epitaxial layers consisting of an asymmetric multiple quantum well (QW) and a GaN-based waveguide with Si- and Mg-doped *n*- and *p*-cladding layers, respectively.[11] The 15-μm-wide emitter strip is located off-center on the top of the chips, which are packed *n* down. The length of the cavity is 1.2 mm. They are housed in a TO56 package; in addition, see the data sheet for the PL TB450B device elsewhere.[12,13] The threshold current I_{th} = 0.15 A (~0.8 kA cm^{-2}), the slope efficiency is 1.6 W A^{-1}, and the emission power at a current of 1.2 A is typically 1.6 W (~8.9 kA cm^{-2}) at a temperature of 25 °C. Eight devices were used

in our study. Electroluminescence (EL) spectra produced with cw or pulsed currents (HP 8114A) were recorded from the front facet of the devices using a Horiba optical grating-based spectrometer and a Bruker Fourier-transform infrared spectrometer equipped with liquid-nitrogen-cooled Ge and HgCdTe detectors. In our experiments, different long- or short-pass filters were used to block specified radiation signals. For comparison, PL was also produced from the GaN substrate using excitations at 442 nm or 457 nm. To avoid excitation-induced thermal effects, the modulated PL (mPL) measured by the step-scan mode of the Fourier-transform infrared spectrometer was produced by chopping the excitation wavelength.[14] Measurements were made at a stable 25 °C using water-cooled Peltier stages or directly at ambient temperature.

Figure 1(a) shows the EL spectra of a GaN-based device in the primary emission range for different cw currents. The typical spontaneous emission (marked by A) of the InGaN QW layer at ~0.03 A is far below I_{th} (= 0.15 A), and the stimulated emission (marked by L) is ~440 nm at ~0.2 A. The inset shows the laser line of ~440 nm at ~0.4 A which is far beyond I_{th}. In addition, besides the spontaneous or stimulated emission centered at ~440 nm, there is a separate emission band peaking at ~550 nm (marked by B).

Figure 1(b) shows the EL for band B after removing the strong emission from the QW with a long-pass filter of 488 nm. For the entire cw-current range (even below I_{th}), band B is always visible and has the same spectral shape. The inset shows the dependence of the integrated intensity of band B on current. It increases linearly at first with a slope of ~1 (in a log–log scale) and then sub-linearly beyond I_{th}. For confirmation, the EL spectrum for an extremely low cw current is also shown without the long-pass filter, which shows that it is possible to record the spontaneous emission (without the stimulated emission) of the device. Indeed, the broad emission from the QW peaks at ~440 nm. There is a half-frequency peak centered at ~880 nm due to the grating-based detection system.

Note that the GaN substrate has abundant defects[8,15] and frequently produces yellow–green band emissions.[16,17] This allows us to attribute band B to the defect-related PL from the GaN substrate. However, Fig. 1(b) shows the PL spectrum of the pure GaN material in the yellow–green region for 442 nm excitation. It is obvious that the PL line shape for GaN is quite similar to that for the device, but the entire spectrum has a red shift (~40 nm). This suggests that band B is an EL signal from defects in the GaN-based QW. The ~40 nm blue shift of the device compared to GaN could result from the quantum confinement of the *optically active region* of the device (i.e., the depletion region of the *pn*-junction, which contains QWs, barriers, and vicinal waveguides), which broadens the emission energy of defect-related transitions. The saturation of the integrated intensity when the current is beyond I_{th}, as shown in the inset, indicates that the emission is caused by the recombination of carriers in the active region. These features of band B are consistent with our previous observations of GaN-based 450 nm devices.[9] Based on spatially resolved measurements of emissions and modeling, the ~580 nm emission band was attributed to the defect-related EL from the optically active region, without any contributions due to PL from the GaN substrate.

Figure 2(a) shows the EL in the SWIR range (as measured by the Ge detector) for different currents. The spectral shape is similar to that of GaN-based 450 nm LDs operated with cw currents[10] and can be tentatively divided into three parts, marked C, D, and E. However, note the weak band E and, more importantly, the emission between bands C and D, as well as the complicated MWIR emission. The figure shows that at a low current of 0.1 A without stimulated emission, bands C and D are not clearly separate, while band E is present. As the current increases to 0.4 A, at which stimulated emission occurs, the EL becomes stronger but with a similar spectral shape. However, the curves have the following differences: (i) band E becomes more distinct without a significant increase in the intensity than bands C and D, and (ii) an absorption-like valley occurs at ~1130 nm (almost corresponding to the absorbance of aqueous vapor but not in the EL spectrum at 0.1 A), making bands C and D more distinct. Please be aware that the mPL spectrum of GaN, which is recorded with a mechanically chopped 457 nm excitation, almost traces the EL spectrum of the device at ~0.1 A [normalized; without an energy shift like that shown in Fig. 1(b)] but not for band E, as shown in Fig. 2(a). This suggests that (i) the SWIR defect emission, including bands C and D, is very likely from the GaN substrate, and (ii) band E may also be related to a genuine defect emission but from a different position from bands C and D although it seems like a thermal-related signal because it is not seen in the mPL spectrum after removing thermal accumulation.

Figure 2(b) shows the EL spectrum of the device at 0.4 A but without the temperature-stabilization system (i.e., the 0.4 A* curve), which means that thermal energy should accumulate in the device. It is obvious that the three emission bands (C–E) are largely

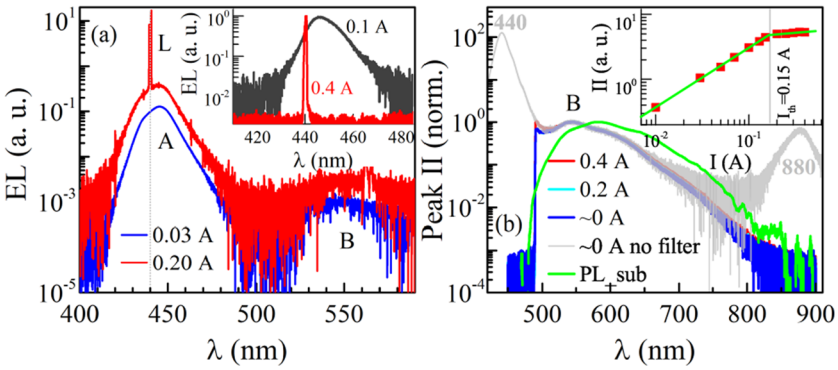

FIG. 1. EL spectra of a device (a) in the primary line range and (b) in the visible-near infrared range for different cw currents. In (a), the inset shows the spontaneous emission and lasing of the device at 0.1 A and 0.4 A. In (b), ~0 A indicates that the extremely low current is close to zero. A 488 nm filter is used to remove the lasing beam. The EL at ~0 A is also shown without the 488 nm filter. The PL from the GaN in this range is produced by 442 nm excitation. The inset shows the dependence of the integrated intensity (II) for band B on the current.

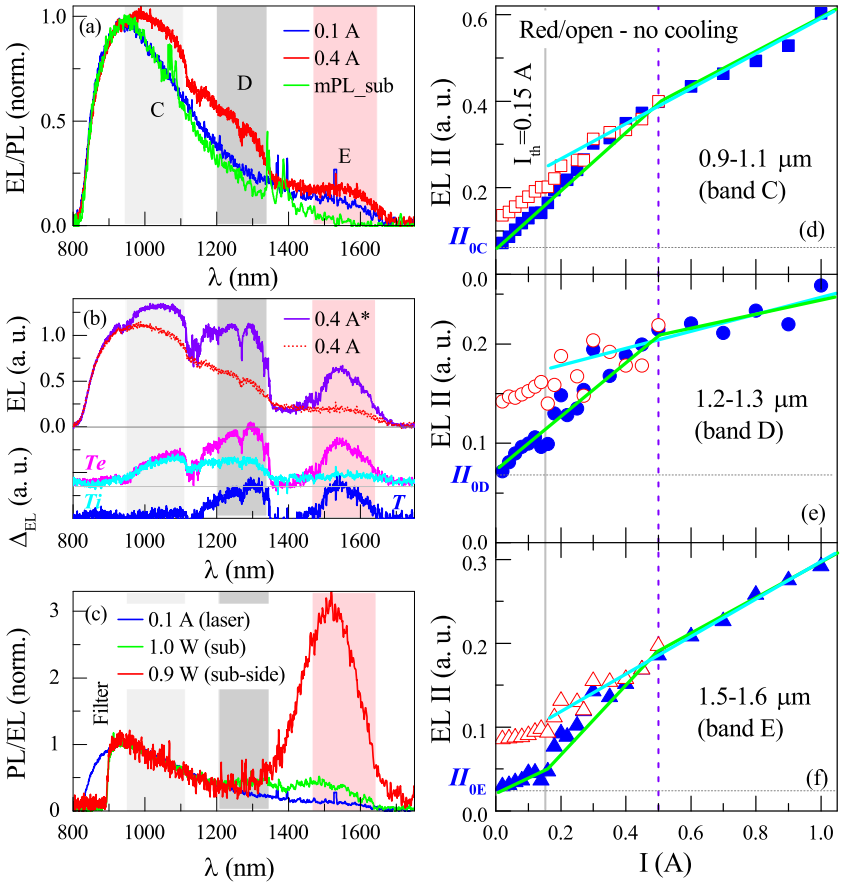

FIG. 2. (a) Normalized EL spectra of the device at 0.1 A and 0.4 A in the SWIR range, together with the mPL spectrum of GaN, (b) EL spectra at 0.4 A and 0.4 A∗, where the 0.4 A∗ emission is measured without the temperature-stabilization system; the curves of T_e, T_i, and T are differences for 0.4 A∗ vs 0.4 A, 0.4 A vs 0.1 A, and T_e vs T_i, respectively, (c) PL spectra of GaN at 457 nm excitation; the excitation spots are focused on the QW growth surface and the side facet of GaN; the EL spectrum of the device at 0.1 A is shown for comparison, and [(d)–(f)] dependence of the integrated intensity on the current for the three EL bands C–E, together with results without the temperature-stabilization system (red open symbols).

strengthened and become more separate, in comparison with the curve at the same current of 0.4 A with the temperature-stabilization system. Thus, the difference between the two spectra, i.e., the T_e curve in the panel, roughly indicates the thermal effect of the device (including the potential emission from defects by thermal activation). As a comparison, the T_i curve shows the difference between the curves 0.4 A and 0.1 A (both with the temperature-stabilization system). For this curve, bands C and D are evidently visible, and band C overlaps the T_e curve. Band E, which can be related to thermal radiation, is extremely weak. This demonstrates that (i) as the current increases up to 0.4 A, the device with a temperature-stabilization system shows no evident thermal accumulation, and (ii) the T_i curve is the real defect emission of the device due to the increase in the current, almost without any contribution from thermal radiation in the SWIR range. Thus, the SWIR emissions, including C, D, and E, must originate from intrinsic deep defects in the device. It can be assumed that the curve T in the panel, which is the difference between the T_e and T_i curves when the temperature-stability system is absent, should be pure thermal radiation due to thermal accumulation. The broad absorption-like valley centered at ~1400 nm is definitely due to aqueous vapor, while the one at ~1130 nm needs further investigation.

Further details of the thermal effects can be seen in Fig. 2(c). The figure shows the PL spectra for different excitation directions for the GaN material, i.e., the surface on which the epilayers are grown and the side facet. The figure shows that due to the high excitation density, band E in the PL spectra is pronounced [but it is not visible in the mPL spectrum shown in Fig. 2(a)] compared to the EL spectrum at 0.1 A, which indicates that there are almost no thermal effects. This suggests that band E, which is from deep defects, can be substantially strengthened by thermal radiation if the (photon/current-induced) temperature effect cannot be effectively reduced in the device. In addition, the thermal accumulation on the side facet of the GaN wafer is much higher than that on the growth facet, even for the lower excitation density. This is also consistent with the anisotropic thermal conductivity of the GaN material,[18] and a heat-transport consideration confirms that the lattice surface chosen for the QW growth has been optimized.[19]

Figures 2(d)–2(f) summarize the dependence of the integrated intensity on the current of the three EL bands, C–E, with (blue solid symbols) and without the temperature-stabilization system (red open symbols). It is evident that all bands, including band E, have a similar evolution, i.e., increasing nearly linearly at first and then sub-linearly after a critical value of $I \approx 0.5$ A. The red open symbols represent the thermal accumulation of the device as long as there is a thermal load during operation. It is clear that at low currents, the red open symbols are substantially higher than the blue

solid symbols, but then they approach each other when the current is above ~0.5 A. By extrapolating the blue solid symbols (with the temperature-stabilization system) to low currents, one can see close agreement with the red open symbols (without the temperature-stabilization system), roughly until I_{th}. These features, including the sub-linear increase beyond 0.5 A of the blue solid symbols with the temperature-stabilization system, can characterize the defect-related emission of the three bands C–E, which can be thermally quenched when the thermal load increases, e.g., beyond 0.5 A. Here, we should again emphasize that even at 0.1 A, where no thermal effect can be expected, band E in the EL spectrum is already evident by referring to the non-zero value at $I = 0$ A, e.g., see II_{0i} (i = E, D, or C) in the panels. This should exclude the main contribution of operation-induced thermal radiation when $I \ll 0.5$ A and leaves only the contribution of the genuine defect-related emission. Notice the transition of the EL integrated intensity of band E at I_{th}, i.e., there is a steeper slope after lasing takes place beyond 0.15 A. This suggests it is different from bands C and D. This may indicate that the defect-related band E makes a larger contribution to the EL (from the optically active region) than to the PL (e.g., bands C and D from the substrate) due to the excitation of the primary spontaneous and stimulated emissions of the device since it cannot be seen in the mPL spectrum for the pure GaN material.

To reveal the thermal effect and its relation with deeper defects, emissions in the MWIR range up to 12 μm were recorded with a dual-channel HgCdTe detector. Figure 3(a) shows the thermal-related radiation of the device for a 1 A cw current with the temperature-stabilization system after subtracting the signal for 0 A (i.e., the room temperature background radiation). This thermal radiation has a peak at ~7.8 μm, which is roughly for a temperature of ~375 K due to the operation-induced thermal accumulation at 1 A, although the temperature-stabilization system was used. The ratio between the 1 A and 0 A curves, as shown in the figure, has a peak at ~4.5 μm with a broad tail down to ~11 μm, which could be for emissions that are not from thermal radiation but from deep defects.

Figure 3(b) shows the dependence of the integrated intensity on the current at ~4.5 μm and ~8.0 μm with or without the temperature-stabilization system. It shows that from the lowest current close to zero, the integrated intensity increases almost linearly at first (which would be more evident in a log–log scale; not shown) but then super-linearly for a critical current of ~0.5 A. This is totally different from the sub-linear behavior in the SWIR range, as shown for band E in Fig. 3(c). However, the critical current of ~0.5 A is almost the same as when using the Ge detector, beyond which the thermal effect governs the emission signal. Taking into account that the linear evolution still occurs when the current is increased across I_{th} and the thermal effect is expected to be small for extremely low currents, we can infer that the linear increase in the emissions below 0.5 A is really from a defect-related EL signal, whereas the super-linear evolution is mainly due to the thermal radiation generated during operation. This assumption is supported by the steeper slope at ~4.5 μm after 0.5 A, which indicates that the signal strengthens at higher temperatures.

Following the discussion above, we can understand that the cw current can lead to the weak thermal effect after I_{th}, but below the critical point of 0.5 A, the effect is drained away by the temperature-stabilization system. To avoid the thermal effect, pulsed currents were used to operate the devices. Figure 4(a) shows the EL spectra for different pulsed currents. The typical pulse width is 1 μs (variable from ~0.1 μs–10 μs). A pulsed width of 1 μs with a pulsed peak of 1 A corresponds to 1 μs A (or 1 μC). Interestingly, when the peak of the pulsed current is increased beyond I_{th}, increased spontaneous emission (or ASE) occurs from SWIR defects. For comparison, EL spectra with cw currents of 0.1 A and 0.4 A are also shown in the figure. It is clear that the ASE peaks at ~1150 nm (marked by a star), almost close to the valley (at ~1130 nm) of the emission spectrum for the 0.4 A cw current. Notice that (i) no evident change in the emission spectral shape is observed in other waveband ranges, e.g., the yellow–green region that is shown in Fig. 1(b), and (ii) pulsed currents can reduce the thermal accumulation. Thus, no thermal radiation contributes to band E. The absence of a red shift of the primary spontaneous emission and, of course, the deep defect-related emission also confirm this hypothesis. This indicates that the primary origin of band E is from intrinsic deep defects, on which the thermal radiation signal is then superimposed.

Figure 4(b) shows the pulsed-current dependence of the SWIR signal that is divided into two parts: one at ~900 nm and the other at ~1150 nm. The ~900 nm signal increases sub-linearly toward saturation and then decreases, while the ~1150 nm signal increases

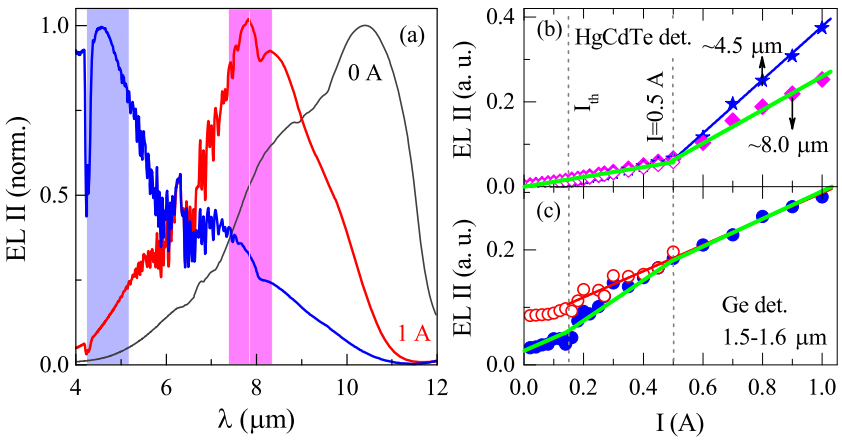

FIG. 3. (a) Normalized thermal-related emission spectra for a 1 A cw current (red) after subtracting the signal for 0 A (gray); the blue line is for a 1 A cw current after dividing by the signal for 0 A, (b) EL integrated intensity vs current in two ranges, ~4.5 μm and ~8.0 μm, and (c) the current dependence of band E for the Ge detector is shown for comparison.

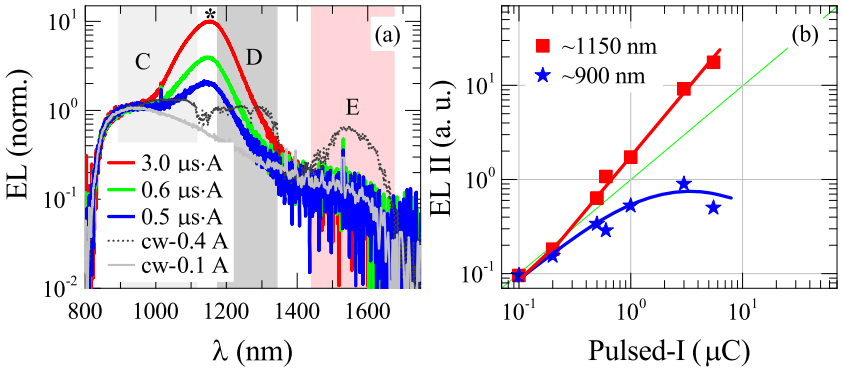

FIG. 4. (a) Representative EL spectra for different pulsed currents; for comparison, the EL spectra for 0.1 A and 0.4 A cw currents are also shown; all curves are normalized to the high-energy side and (b) dependence of the integrated intensity on the pulsed current for the EL at ~900 nm and ~1150 nm in a log–log scale.

super-linearly (i.e., ASE) as the pulsed current increases. Notice that (i) different pulse widths and repetition rates have been used, which give a similar evolution of the two emission parts, (ii) the data shown in Fig. 4(b) are recorded at the same repetition rate of ~40 kHz, which ensures the full-recombination/relaxation of the non-equilibrium carriers after each pulse, and (iii) more importantly, the ASE can hardly be seen when the pulsed current is below I_{th}. This suggests that (i) the data in Fig. 4(b) are comparable and convincing even if there are slight changes in the pulse width and the pulsed peak current, and (ii) this SWIR defect-related ASE could be from deep defects in the optically active region, as an accompaniment to the stimulated emission from the InGaN QW of the device.

Note that the spontaneous emission from the SWIR defects observed for the cw currents can be amplified as ASE with pulsed currents only if the pulsed peak current is beyond I_{th}. The main difference between pulsed and cw currents is that the former prevents thermal accumulation in the optically active region, especially in the QW. In other words, a pulsed current significantly reduces the non-radiative recombination of the non-equilibrium carriers in the optically active region. Further, it enhances the lasing of the InGaN QWs and promotes the radiative recombination of the non-equilibrium carriers in the deep defects. In the resonance cavity, the defect-related spontaneous emission is amplified. As discussed above, for cw currents, the SWIR emission, including the range of ~1130 nm–1160 nm, is dominated by the PL signal from the GaN substrate. Thus, the ASE peak at ~1150 nm could mainly be due to EL from deep defects in the InGaN QWs, with a minor contribution from PL due to the excitation of the primary lasing line (440 nm) in the deep defects in the device, including in the InGaN QWs and the GaN substrate since the peak can be observed only when the pulsed current is beyond I_{th}. Then, the valley at ~1130 nm for cw currents, which is the PL signal from the GaN substrate, may be due to two factors: (i) the absorption of the aqueous vapor and (ii) the extraction of carriers from the deep defects, resulting in stimulated emission in the InGaN QWs when the cw current is beyond I_{th}. This observed ASE also suggests that the SWIR defects have a key detrimental influence on the devices since they consume the non-equilibrium carriers, either as a radiative recombination signal or as a thermal-accumulated radiation signal.

We should emphasize that the IR emissions investigated in our work are small in power compared to laser emissions. Experimental estimations using optical density filters lead to the conclusion that all IR-emissions together account for less than 10^{-3} of the primary power of the laser. In numbers, this means that there is less than ~1 mW of IR emissions at 1.6 W output power. Therefore, the loss of quantum yield caused by the IR emission is rather small. Nevertheless, it is important to pay attention to the IR emissions when practically applying such diode lasers, especially, for example, in metrology or analytics, where these emissions can falsify the results. In addition, we point out that even IR emissions can be optically amplified. If such effects are strongly pronounced, this could even become a relevant loss mechanism.

In summary, we have analyzed broad emission bands for defects in 440-nm-emitting (In,Ga,Al)N LDs operated with cw and pulsed currents. In addition to the primary spontaneous and stimulated emission, the defect-related yellow–green band, and the SWIR band, the defect emission can even extend into the MWIR band. Moreover, the thermal radiation can be separately detected and identified. Consistent with our previous work, the yellow–green emission is the EL signal from defects in the active area (QWs and waveguide) under the emitter stripe. The SWIR emission, however, is complicated. On the short wavelength side, it is mainly due to the PL signal from deep defects in the GaN substrate (e.g., below ~1000 nm), whereas on the long wavelength side (beyond ~1400 nm), it is due to EL from the optically active region, which is superimposed on the thermal radiation. The special middle part (1000 nm–1400 nm) is generated in the GaN substrate by photo-excitation in deep-level defects by spontaneous primary emission for cw currents. For pulsed currents, the EL due to defects in the optically active region dominates and produces an ASE peak at ~1150 nm. These results reveal the key detrimental influence of the SWIR deep defects on the non-equilibrium carriers in GaN-based devices. Further investigations on how to prevent these defects are important for improving the efficiency and stability of these devices.

AUTHOR'S CONTRIBUTIONS

F.M. and J.H. contributed equally to this work.

ACKNOWLEDGMENTS

The authors thank the National Natural Science Foundation of China (Grant Nos. 61874043, 61790583, 61874045, and 61775060)

and the Aero-Science Fund (Grant No. 201824X8001) for their financial support.

DATA AVAILABILITY

The data that support the findings of this study are available from the corresponding author upon reasonable request.

REFERENCES

[1]T. D. Moustakas and R. Paiella, Rep. Prog. Phys. **80**, 106501 (2017).
[2]G. Wang, F. Chong, C. Xiong, J. Wang, Y. Zhao, S. Liu, and X. Ma, J. Opt. Laser **20**, 1310 (2009).
[3]Z. Zhao, A. Singh, J. Chesin, R. Armitage, I. Wildeson, P. Deb, A. Armstrong, K. Kisslinger, E. A. Stach, and S. Gradečak, Appl. Phys. Express **12**, 034003 (2019).
[4]S. J. Sweeney, L. J. Lyons, A. R. Adams, and D. A. Lock, IEEE J. Sel. Top. Quantum Electron. **9**, 1325 (2003).
[5]H. Imai, K. Isozumi, and M. Takusagawa, Appl. Phys. Lett. **33**, 330 (1978).
[6]M. Hempel, J. W. Tomm, F. Yue, M. A. Bettiati, and T. Elsaesser, Laser Photonics Rev. **8**, L59 (2014).
[7]M. Ziegler, R. Pomraenke, M. Felger, J. W. Tomm, P. Vasa, C. Lienau, M. B. Sanayeh, A. Gomez-Iglesias, M. Reufer, F. Bugge, and G. Erbert, Appl. Phys. Lett. **93**, 041101 (2008).
[8]M. Sumiya, S. Ueda, K. Fukuda, Y. Asai, Y. Cho, L. Sang, A. Uedono, T. Sekiguchi, T. Onuma, and T. Honda, Appl. Phys. Express **11**, 021002 (2018).
[9]R. Kernke, H. Wang, J. Hong, F. Yue, J. Chu, and J. W. Tomm, OSA Continuum **2**, 1496 (2019).
[10]R. Kernke, M. Hempel, J. W. Tomm, T. Elsaesser, B. Stojetz, H. König, and U. Strauss, Opt. Mater. Express **6**, 2139 (2016).
[11]G. Mura, M. Vanzi, M. Hempel, and J. W. Tomm, Phys. Status Solidi RRL **11**, 1700132 (2017).
[12]See https://www.lasershop.de/laserquellen/laserdioden/blaue-laserdioden-405nm-445nm-450nm-460nm/ for the information of the products.
[13]See https://www.osram.com/os/ecat/Metal%20Can%C2%AE%20TO56%20PL%20TB450B/com/en/class_pim_web_catalog_103489/global/prd_pim_device_2220053/ for the data sheet of the PL TB450B device.
[14]J. Shao, W. Lu, X. Lü, F. Yue, Z. Li, S. Guo, and J. Chu, Rev. Sci. Instrum. **77**, 063104 (2006).
[15]M. Sumiya, N. Toyomitsu, Y. Nakano, J. Wang, Y. Harada, L. Sang, T. Sekiguchi, T. Yamaguchi, and T. Honda, APL Mater. **5**, 016105 (2017).
[16]K. Motoki, SEI Tech. Rev. **70**, 28 (2010).
[17]T. Langer, A. Kruse, F. A. Ketzer, A. Schwiegel, L. Hoffmann, H. Jönen, H. Bremers, U. Rossow, and A. Hangleiter, Phys. Status Solidi C **8**, 2170 (2011).
[18]W. Ju, Z. Zhou, and Z. Wei, AIP Adv. **6**, 065328 (2016).
[19]A. R. Arehart, A. Corrion, C. Poblenz, J. S. Speck, U. K. Mishra, and S. A. Ringel, Appl. Phys. Lett. **93**, 112101 (2008).